

Decoherence effects on local quantum Fisher information and quantum coherence in a spin-1/2 Ising-XYZ chain

Hector L. Carrion¹, Onofre Rojas², Cleverson Filgueiras², Moises Rojas²

¹*School of Science and Technology, Federal University of Rio Grande do Norte, 59078-900, Natal-RN, Brazil, and*

²*Department of Physics, Institute of Natural Science, Federal University of Lavras, 37200-900, Lavras-MG, Brazil*

This research explores the effects of decoherence on local quantum Fisher information (LQFI) and quantum coherence dynamics in a spin-1/2 Ising-XYZ chain model with independent reservoirs at zero temperature. Contrasting these effects with those in the spin-1/2 Heisenberg XYZ model reveals intricate interactions among quantum coherence, entanglement, and environmental decoherence in spin systems. Analysis of coherence dynamics highlights differences between the original and hybrid models, showcasing increased entanglement due to Ising interactions alongside reduced coherence from environmental redistribution. LQFI proves more resilient than coherence in specific scenarios, emphasizing decoherence's varying impacts on quantum correlations. This research underscores the complexity of quantum coherence dynamics and the crucial role of environmental factors in shaping quantum correlations, providing insights into entanglement and coherence behavior under environmental influences and guiding future studies in quantum information processing and correlation dynamics.

PACS numbers:

I. INTRODUCTION

The quantum resource theories [1–3] play a crucial role in the quantum information processing, specifically in the domains of, quantum communication and quantum computation [4, 5]. These theories identify quantum coherence and entanglement as two fundamental resources. Notably, the most fascinating nonlocal correlation is the quantum entanglement, an intriguing form of correlation, is widely recognized as a vital physical resource for quantum computation and quantum information. As the natural candidates for the realization of the quantum coherence, spin chains systems can be used to understand the evolution of the quantum coherence in its different partitions. Recently, there has been extensive research on the Heisenberg model in the field of condensed matter [6–8]. The influence of quantum coherence on Heisenberg spin models have been considerable investigated [9–11]. Moreover, recent studies reveal a close connection between these resources [12].

The Heisenberg spin diamond chain is a kind of important and interesting model, but the rigorous theoretical treatment is very difficult task due to a non-commutability of spin operators. To overcome problem, a novel class of the simplified versions of the so-called Ising-Heisenberg diamond chain was introduced in Ref. [13]. Lately, the properties of thermal entanglement have been studied in several Ising-Heisenberg on diamond chain [14–17]. In addition, Rojas *et al* [18] discussed the entangled state teleportation through a couple of quantum channels composed of XXZ dimers in an Ising- XXZ diamond chain. More recently, the effects of impurity embedded in an Ising-Heisenberg diamond chain on quantum coherence and quantum teleportation have been reported [19–21].

Recently, a novel measure called local quantum Fisher information (*LQFI*) [22, 23] has emerged for quantify non-classical correlations through quantum Fisher information (*QFI*). This powerful quantifier, akin to quantum discord, involves minimizing *QFI* through a locally informative observable linked to a specific subsystem. Furthermore, *LQFI* holds significant promise as a tool to elucidate the influence of quantum correlations, extending beyond entanglement, and enhancing the precision and efficiency of quantum estimation protocols.

On the other hand, it is widely recognized that realistic quantum systems inevitably interact with their environment, leading to decoherence, which represents a fundamental challenge in quantum information processing [24–27]. Therefore, the investigation of essential aspects regarding the dynamic behavior of quantum coherence under decoherence has drawn significant interest in recent years [28–33]. In recent years, extensive research has explored the dissipative effects on the dynamics of quantum correlations in Heisenberg spin chains, analyzing scenarios both in the presence and absence of an external magnetic field [34–37]. Therefore, it is crucial to continue investigating the study of quantum correlations within spin models subject to decoherence.

In this paper, based on the previously mentioned developments, we conducted a comprehensive investigation into the effects of Ising spins on the dynamics of quantum coherence within the Ising-XYZ spin model. This study was conducted under the influence of environmental decoherence at zero temperature and in the presence affect of an inhomogeneous magnetic field. The dynamics are modeled using the Lindblad master equation [24], from which we derived analytical solutions. These solutions

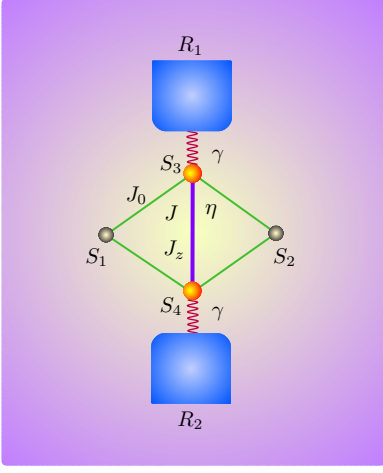


FIG. 1: (Color online) A schematic representation of structure of the Ising-XYZ spin chain model with diamond structure connected with two independent baths R_1 and R_2 at zero temperature. The large (orange) circles are the Heisenberg spins, while small (gray) circles are the Ising spins.

enable us to explore in detail the concurrence and the behavior of the l_1 -norm of coherence. Additionally, our analysis allows for the investigation of the dynamics of the local quantum Fisher information.

Our paper is structured as follows. In Sec. II, we introduce the hybrid Ising-XYZ model and derive the Markovian master equation describing the dynamics of the system. In Sec. III, we provide an overview on concurrence, quantum coherence and local quantum Fisher information to quantify the degree of quantum correlations presented in a spin-1/2 Ising-XYZ chain. In Sec. IV, we discuss some of the most interesting results of the dynamics of entanglement, quantum coherence, and local quantum Fisher information of the model studied. Finally, our conclusion is given in Sec. V.

II. THE MODEL AND MASTER EQUATION

In this section, we present the Hamiltonian describing the spin-1/2 Ising-XYZ model on a diamond chain subjected to an external inhomogeneous magnetic field. The model consists of interstitial Heisenberg spins (S_3^i, S_4^i) and Ising spins (S_1^z, S_2^z) located in the nodal site, as illustrated in Fig. 1. The total Hamiltonian of the model may be written as

$$\begin{aligned} \mathcal{H} = & J(1+\eta)S_3^xS_4^x + J(1-\eta)S_3^yS_4^y + J_zS_3^zS_4^z \\ & + J_0(S_1^z + S_2^z)(S_3^z + S_4^z) \\ & + (B+b)S_3^z + (B-b)S_4^z + \frac{B}{2}(S_1^z + S_2^z). \end{aligned} \quad (1)$$

Here, J and J_z represent the XYZ interaction within the Heisenberg dimer, while η denotes XY-anisotropy parameter. The nodal-interstitial spins interaction are represented by the Ising-type exchanges J_0 . Additionally, B denotes the longitudinal uniform magnetic field in

the z direction and b corresponds to the longitudinal nonuniform magnetic field in the same direction. The matrix form of the Hamiltonian \mathcal{H} is given by

$$\mathcal{H} = \begin{bmatrix} \mathcal{H}_1 & \mathbf{0} & \mathbf{0} & \mathbf{0} \\ \mathbf{0} & \mathcal{H}_0 & \mathbf{0} & \mathbf{0} \\ \mathbf{0} & \mathbf{0} & \mathcal{H}_0 & \mathbf{0} \\ \mathbf{0} & \mathbf{0} & \mathbf{0} & \mathcal{H}_{-1} \end{bmatrix}.$$

Here, we have three distinct blocks: \mathcal{H}_1 corresponds to the z -component of spins ($S_1^z = S_2^z = +1/2$), \mathcal{H}_0 corresponds to the z -component of spins ($S_1^z = \pm 1/2, S_2^z = \mp 1/2$) and \mathcal{H}_{-1} corresponds to the z -component of spins ($S_1^z = S_2^z = -1/2$).

After diagonalization, the eigenvalues for the XYZ dimer of the Hamiltonian \mathcal{H}_μ can be obtained as follows

$$\begin{aligned} \mathcal{E}_{1,4} &= \frac{B\mu}{2} + \frac{J_z}{4} \pm \frac{\Omega}{2}, \\ \mathcal{E}_{2,3} &= \frac{B\mu}{2} - \frac{J_z}{4} \pm \frac{\omega}{2}, \end{aligned}$$

where $\Omega^2 = J^2\eta^2 + 4\Delta^2$, $\omega^2 = J^2 + 4b^2$, $\Delta = J_0\mu + B$ and $\mu = S_1^z + S_2^z$. Note that \mathcal{E} depends on μ .

In this paper μ is the control parameter of the possible values of the Ising type spins, where μ assumes the values $\{0, \pm 1\}$. Here $\mu = 0$ corresponding the antiferromagnetic case and $\mu = \pm 1$ corresponding the ferromagnetic case. We consider the convention $|0\rangle = |\uparrow\rangle$ and $|1\rangle = |\downarrow\rangle$ to indicate the spin-up and spin-down respectively.

By assuming that the spins S_3 and S_4 of the system interacts independently with the environment, and considering weak system-reservoir coupling as well as the Born-Markov approximation [24], the dynamics of the dissipative system can be described by master equation, which can be written most generally in the Lindblad form ($\hbar = 1$). Thus, for our specific case, the Lindblad equation takes the following form

$$\frac{d\rho}{dt} = -i[\mathcal{H}, \rho] + \sum_{j=3,4} \gamma \left[S_j^- \rho S_j^+ - \frac{1}{2} \{S_j^+ S_j^-, \rho\} \right], \quad (2)$$

where $\{, \}$ denotes the anticommutator, and γ represents the environmental decoherence rate. Here ρ is the density operator of the model. We assume that initially the system's density matrix has the so-called X form, which is preserved during the evolution according to the master equation Eq. (2). In the standard basis $\{|00\rangle, |01\rangle, |10\rangle, |11\rangle\}$, we have

$$\rho_\mu(t) = \begin{bmatrix} \rho_{11}(t) & 0 & 0 & \rho_{14}(t) \\ 0 & \rho_{22}(t) & \rho_{23}(t) & 0 \\ 0 & \rho_{32}(t) & \rho_{33}(t) & 0 \\ \rho_{41}(t) & 0 & 0 & \rho_{44}(t) \end{bmatrix},$$

with $\rho_{41}(t) = \rho_{14}^*(t)$, $\rho_{32}(t) = \rho_{23}^*(t)$.

So, the density operator of the model has the following structure

$$\rho(t) = \begin{bmatrix} \rho_1(t) & \mathbf{0} & \mathbf{0} & \mathbf{0} \\ \mathbf{0} & \rho_0(t) & \mathbf{0} & \mathbf{0} \\ \mathbf{0} & \mathbf{0} & \rho_0(t) & \mathbf{0} \\ \mathbf{0} & \mathbf{0} & \mathbf{0} & \rho_{-1}(t) \end{bmatrix}.$$

We further suppose that the interacting of the two-qubit Ising- XYZ model with the environment is undergo dephasing process.

The master equation provided in Eq. (2) is equivalent to a system of coupled differential equations. These equations can be solved assuming $|\Psi\rangle = \sin\theta|01\rangle + \cos\theta|10\rangle$ as the initial state, resulting in the following expressions

$$\begin{aligned}\rho_{11} &= \frac{J^2\eta^2[\Omega(1-e^{-2\gamma t})-2\gamma\sin(\Omega t)e^{-\gamma t}]}{4\Omega(\Omega^2+\gamma^2)}, \\ \rho_{22} &= \frac{[J(2b\sin 2\theta-J\cos 2\theta)\cos(\omega t)]e^{-\gamma t}}{2\omega^2} \\ &\quad - \frac{[2\Omega^2b^2\cos 2\theta+\Omega^2Jb\sin 2\theta-2\Delta^2\omega^2]e^{-\gamma t}}{\Omega^2\omega^2} \\ &\quad + \frac{J^2\eta^2\gamma^2\cos(\Omega t)e^{-\gamma t}}{2\Omega^2(\Omega^2+\gamma^2)} + \frac{J^2\eta^2(1+e^{-2\gamma t})}{4(\Omega^2+\gamma^2)}, \\ \rho_{33} &= \frac{[J(J\cos 2\theta-2b\sin 2\theta)]\cos(\omega t)e^{-\gamma t}}{2\omega^2} \\ &\quad + \frac{[2\Omega^2b^2\cos 2\theta+\Omega^2Jb\sin 2\theta+2\Delta^2\omega^2]e^{-\gamma t}}{\Omega^2\omega^2} \\ &\quad + \frac{J^2\eta^2\gamma^2\cos(\Omega t)e^{-\gamma t}}{2\Omega^2(\Omega^2+\gamma^2)} + \frac{J^2\eta^2(1+e^{-2\gamma t})}{4(\Omega^2+\gamma^2)}, \\ \rho_{44} &= \frac{J^2\eta^2\gamma[\Omega\sin(\Omega t)-2\gamma\cos(\Omega t)]e^{-\gamma t}}{2\Omega^2(\Omega^2+\gamma^2)} \\ &\quad - \frac{4\Delta^2e^{-\gamma t}}{\Omega^2} + \frac{-J^2\eta^2e^{-2\gamma t}+\Omega^2+12\Delta^2+4\gamma^2}{4(\Omega^2+\gamma^2)}, \\ \rho_{23} &= \frac{-(J\cos 2\theta-2b\sin 2\theta)[i\omega\sin(\omega t)+2b\cos(\omega t)]e^{-\gamma t}}{2\omega^2} \\ &\quad + \frac{J(J\sin 2\theta+2b\cos 2\theta)e^{-\gamma t}}{2\omega^2}, \\ \rho_{14} &= \frac{J\eta\gamma[(i\gamma+2\Delta)\Omega\sin(\Omega t)+(i\Omega^2-2\gamma\Delta)\cos(\Omega t)]e^{-\gamma t}}{2\Omega^2(\Omega^2+\gamma^2)} \\ &\quad + \frac{J\eta[2\Delta(\Omega^2+\gamma^2)e^{-\gamma t}-(i\gamma+2\Delta)\Omega^2]}{2\Omega^2(\Omega^2+\gamma^2)}.\end{aligned}$$

III. DYNAMICS OF QUANTUM CORRELATIONS

In this section, we will focus on studying the dynamics of the entanglement, quantum coherence and local quantum Fisher information. Specifically, we aim to investigate the entanglement dynamics of anisotropic Heisenberg qubits on the Ising- XYZ model. To accomplish this, we will utilize the concurrence \mathcal{C} as a measure of entanglement, as defined by [38, 39]

$$\mathcal{C}(\rho) = \max\{\sqrt{\lambda_1} - \sqrt{\lambda_2} - \sqrt{\lambda_3} - \sqrt{\lambda_4}, 0\}, \quad (3)$$

where λ_i ($i = 1, 2, 3, 4$) are the eigenvalues in a decreasing order of the operator R , which is given by

$$R = \rho \cdot (\sigma^y \otimes \sigma^y) \cdot \rho^* \cdot (\sigma^y \otimes \sigma^y). \quad (4)$$

ρ^* denotes the complex conjugate of matrix ρ . In our model, the concurrence for a state of the form given by Eq. (3) is given by

$$\mathcal{C} = 2\max\{|\rho_{23}| - \sqrt{|\rho_{11}\rho_{44}|}, |\rho_{14}| - \sqrt{|\rho_{22}\rho_{33}|}, 0\}. \quad (5)$$

On the other hand, the quantum coherence is a useful resource for the quantum information processing task. Here, we will employ the l_1 -norm[40] measure, defined as

$$C_{l_1}(\rho) = \sum_{i \neq j} |\rho_{ij}|.$$

The corresponding l_1 -norm of the quantum coherence of the impure dimer described by the reduced density operator, $\rho(t)$, is given by

$$C_{l_1} = 2|\rho_{2,3}| + 2|\rho_{1,4}|. \quad (6)$$

It is worth noting that quantum coherence is a basis-dependent concept. To analyze \mathcal{C}_{l_1} , we perform a unitary transformation on the density matrix of the bipartite system ρ_{AB} . The transformed density matrix is given by $\tilde{\rho}_{AB} = \tilde{U}\rho_{AB}\tilde{U}^\dagger$, where $\tilde{U} = U \otimes U$. The unitary matrix U is defined as

$$U = \begin{bmatrix} \cos\phi & -e^{i\varphi}\sin\phi \\ e^{-i\varphi}\sin\phi & \cos\phi \end{bmatrix}. \quad (7)$$

The quantum Fisher information is essential in quantum estimation theory, serving as the quantum equivalent of classical Fisher information. This quantifier provides us with a profound understanding of how quantum correlations play a crucial role in determining metrological precision. Specifically, when $\rho_\theta = e^{-i\theta H}\rho e^{i\theta H}$, where H is a fixed Hermitian operator on the system ρ , the quantum Fisher information becomes independent of the estimated parameter θ [41, 42].

$$\mathcal{F}(\rho, H) = \frac{1}{2} \sum_{i \neq j} \frac{(p_i - p_j)^2}{p_i + p_j} |\langle \psi_i | H | \psi_j \rangle|^2, \quad (8)$$

where $p_i(p_j)$ and $|\psi_i\rangle$ ($|\psi_j\rangle$) are the eigenvalues and eigenvectors, respectively, of the density matrix ρ . Now, assuming that the dynamics is governed by local Hamiltonian $H = H_A \otimes \mathbb{I}$, with H_A defined as $H_A = \boldsymbol{\sigma} \cdot \mathbf{r}$, where $|\mathbf{r}| = 1$ and $\boldsymbol{\sigma}$ is the Pauli spin vectors, we can derive the quantification of quantum correlations in terms of local quantum Fisher information ($LQFI$) as follows

$$\mathcal{Q}_{\mathcal{F}} = 1 - \lambda_{max}^{\mathcal{M}}, \quad (9)$$

where $\lambda_{max}^{\mathcal{M}}$ denotes the largest eigenvalue of the symmetric matrix \mathcal{M} with elements

$$\mathcal{M}_{lk} = \sum_{i \neq j} \frac{2p_i p_j}{p_i + p_j} \langle \psi_i | \sigma_l \otimes \mathbb{I} | \psi_j \rangle \langle \psi_j | \sigma_k \otimes \mathbb{I} | \psi_i \rangle. \quad (10)$$

IV. RESULTS AND DISCUSSION

In this section, we outline the main results regarding the dynamical of concurrence, quantum coherence, and local quantum Fisher information for the spin-1/2 Ising- XYZ chain.

A. Concurrence

In the following, we compare the time evolution of entanglement between the original spin-1/2 Heisenberg

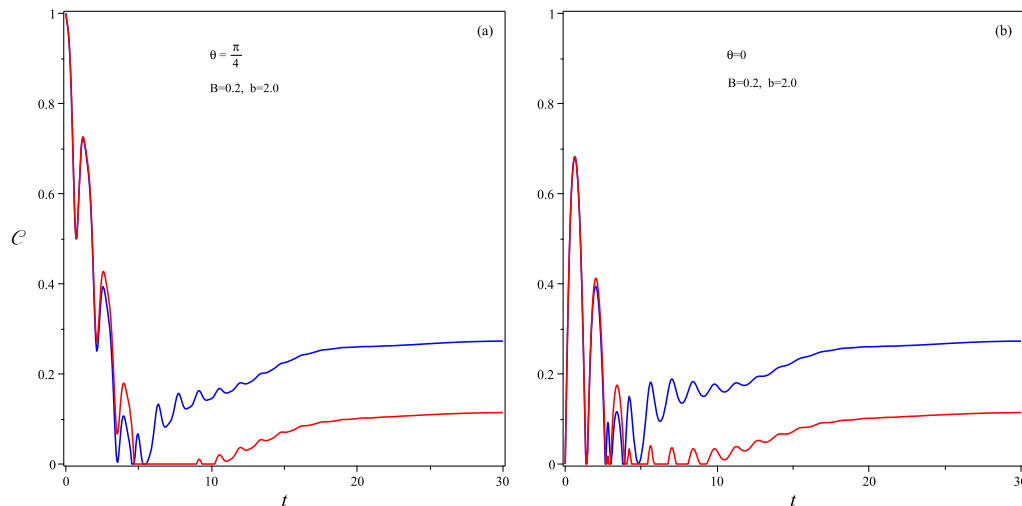


FIG. 2: (Color online) The concurrence \mathcal{C} as a function of time t , with $J = 2.0$, $J_0 = 1.0$, $\gamma = 0.2$, $\eta = 0.2$. Here, the blue curve corresponds to two-qubit Heisenberg XYZ model and red curve corresponds to two-qubit Ising- XYZ model. (a) $\theta = \frac{\pi}{4}$. (b) $\theta = 0$.

XYZ model [37] and the hybrid spin-1/2 Ising- XYX model. In this case, the two-qubits system is initially prepared in the state $|\Psi\rangle = \sin\theta|01\rangle + \cos\theta|10\rangle$. In Fig. 2, the concurrence \mathcal{C} , as a function of the time t is depicted for $J = 2.0$, $J_0 = 1.0$, $\gamma = 0.2$, $\eta = 0.2$, $B = 0.2$, $b = 2.0$, and for various values of the parameter θ . Here, the red curve represents the concurrence for the Heisenberg model, while the blue curve represents the concurrence for the Ising- XYZ chain. Thus, in Fig. 2(a), we display the concurrence \mathcal{C} for initial state $|\Psi\rangle = \frac{1}{\sqrt{2}}(|01\rangle + |10\rangle)$, which is maximally entangled ($\theta = \pi/4$). We can observe that the concurrence for the Ising- XYZ model is slightly more robust than in the original model until reaching the first entanglement sudden death (ESD), after which there is a reversal in entanglement efficiency. In this region, entanglement is notably more robust in the original model than in the Ising- XYZ spin chain model. On the other hand, we are also interested in the behavior of concurrence when the initial state is completely non-entanglement. Thus, in Fig. 2(b), we depict the concurrence for the initially unentangled state $|\Psi\rangle = |01\rangle$ ($\theta = 0$). It is easy to see that we have three well-defined regions of concurrence behavior. In the initial sector, one can observe that initially the concurrence is null for both models and for short time intervals, the concurrence of the original model and hybrid models is similar. However, in this region, the hybrid model (red curve) is slightly more robust than the original model (blue curve). In the second sector, there is a significant change in the concurrence behavior. In this region, both models experience entanglement sudden death (ESD) and entanglement sudden birth (ESB) in a short time [43, 44]. Finally, in the last sector, the entanglement of the models grows progressively, with the predominance of the Heisenberg model's over the Ising-

XYZ model. Ultimately, the concurrence for each model reaches a steady state after exhibiting some oscillatory behavior.

In the following, we study the population dynamic of the hybrid Ising- XYZ diamond chain. Fig. 3 illustrates the dynamics of population ρ_{ii} ($i = 1, 2, 3, 4$) for the initial state $|\Psi\rangle = \sin\theta|01\rangle + \cos\theta|10\rangle$, with specific emphasis on states corresponding for $\theta = \pi/4$ and $\theta = 0$. In both cases we fixed the parameters $J = 2.0$, $J_0 = 1.0$, $\gamma = 0.2$, $\eta = 0.2$. Specifically, Fig. 3(a) show the evolution of population dynamics for the entanglement state ($\theta = \frac{\pi}{4}$). On a short-time scale, the population ρ_{22} (red curve) and ρ_{33} (green curve) corresponding to Bell state exhibit fast oscillations. Notably, the populations of ρ_{11} (black curve) and ρ_{44} (blue curve), which were initially zero, experience a rapid increase for ρ_{44} , while the population associated with ρ_{11} exhibits a slower increment. Fig. 3(b) corresponds to the case when the system is initially prepared in the unentangled state $|\Psi\rangle = |10\rangle$ ($\theta = 0$). Similarly to case in Fig. 3(a), it is observed here that the initially zero populations of ρ_{44} increase rapidly, while the population corresponding to ρ_{11} shows a slower increment. On the other hand, it is evident that the system starts in the state ρ_{33} . As time progresses, the state ρ_{22} and ρ_{33} undergo a series of oscillations, culminating in the emergence of quantum entanglement (see Fig. 2(b)) due to interaction with the environment.

In Fig. 4, we conducted a more in-depth analysis of the dynamics of concurrence (Eq.5) shows in the Figure 2(a), nothing that it consists of two distinct parts, \mathcal{C}_1 and \mathcal{C}_2 . Regarding $\mathcal{C}_1 = 2\max\{|\rho_{23}| - \sqrt{\rho_{11}\rho_{44}}, 0\}$ (red curve), we identified a competition between the initial state $|\Psi\rangle = \sin\theta|01\rangle + \cos\theta|10\rangle$ associate with ρ_{23} and populations ρ_{11} and ρ_{44} , which then abruptly disappear, expected to generate entanglement in the reservoirs. After a period

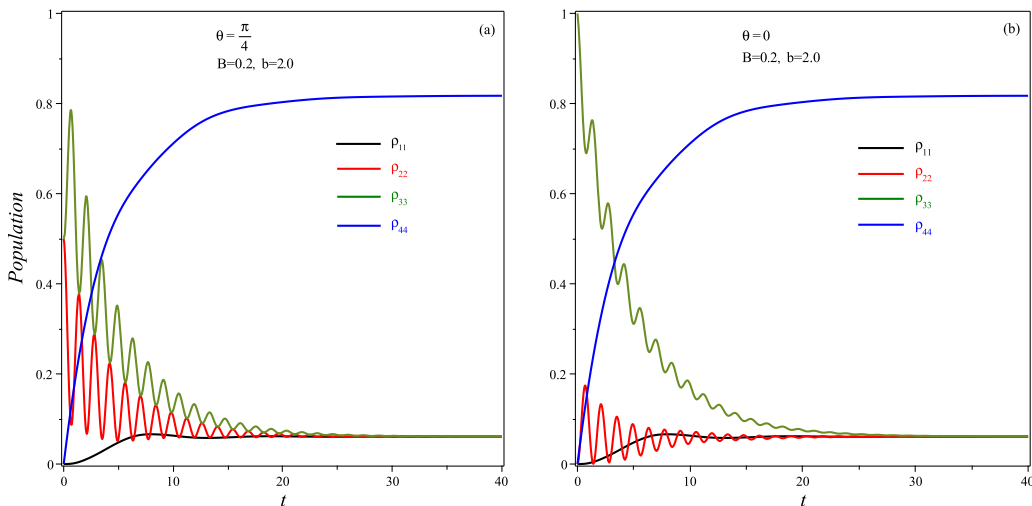


FIG. 3: (Color online) The population as a function of time t for Ising-XYZ model. (a) $\theta = \frac{\pi}{4}$. (b) $\theta = 0$. The parameters are chosen as $J = 2.0$, $J_0 = 1.0$, $\gamma = 0.2$, $\eta = 0.2$.

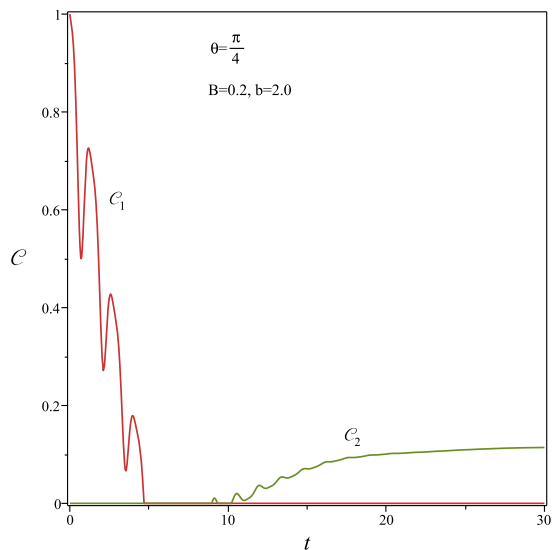


FIG. 4: (Color online) Concurrence \mathcal{C}_1 and \mathcal{C}_2 plotted against time t for the Ising-XYZ chain with $B = 0.2$, $b = 2.0$. The other parameters are set to $J = 2.0$, $J_0 = 1.0$, $B = 0.2$, $\gamma = 0.2$, $\eta = 0.2$ and $\theta = \pi/4$.

of time without entanglement presence, a sudden birth of entanglement, $\mathcal{C}_2 = 2\max\{|\rho_{14}| - \sqrt{\rho_{22}\rho_{33}}, 0\}$ (green curve), occurs as a result of interaction with the environment. Surprisingly, this quantum entanglement is generated by the state ρ_{14} , contrasting with the initial entanglement associated with the state ρ_{23} . In Fig. 5, we show the behavior of the concurrence \mathcal{C} as a function of time t and b , with $\theta = \frac{\pi}{4}$. The figure reveals that near $b = 1$, there is a narrow region characterized by abrupt events of entanglement sudden death and entanglement sudden birth around $t = 3$. For $t > 5$, a broad area

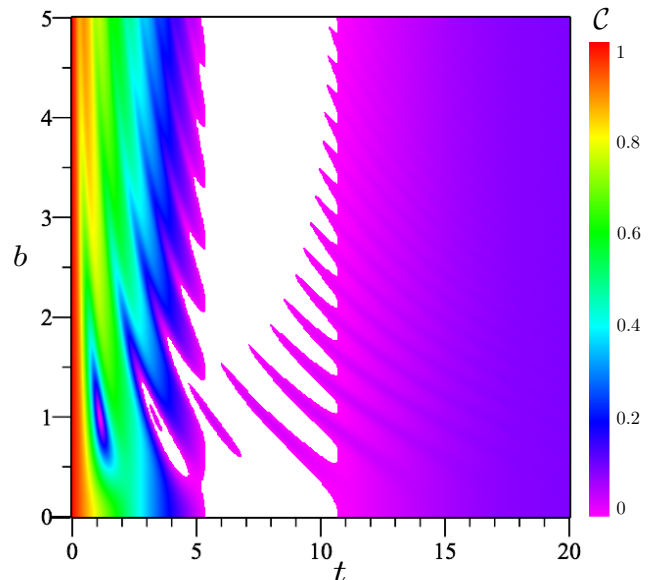


FIG. 5: (Color online) Density plot of concurrence \mathcal{C} as a function of time t and magnetic field b . The parameters are chosen as $J = 2.0$, $J_0 = 1.0$, $B = 0.2$, $\gamma = 0.2$, $\eta = 0.2$ and $\theta = \pi/4$.

emerges where entanglement dissipates and re-emerges recurrently, clearly indicating the dynamic interaction between the system and environment [27]. White regions indicate where the system is entirely unentangled.

B. The l_1 -norm of coherence

To illustrate the behavior of quantum coherence in our model, the l_1 -norm of coherence \mathcal{C}_{l_1} versus the time t is plotted in Fig. 6 for the magnetic fields $B = 0.2$

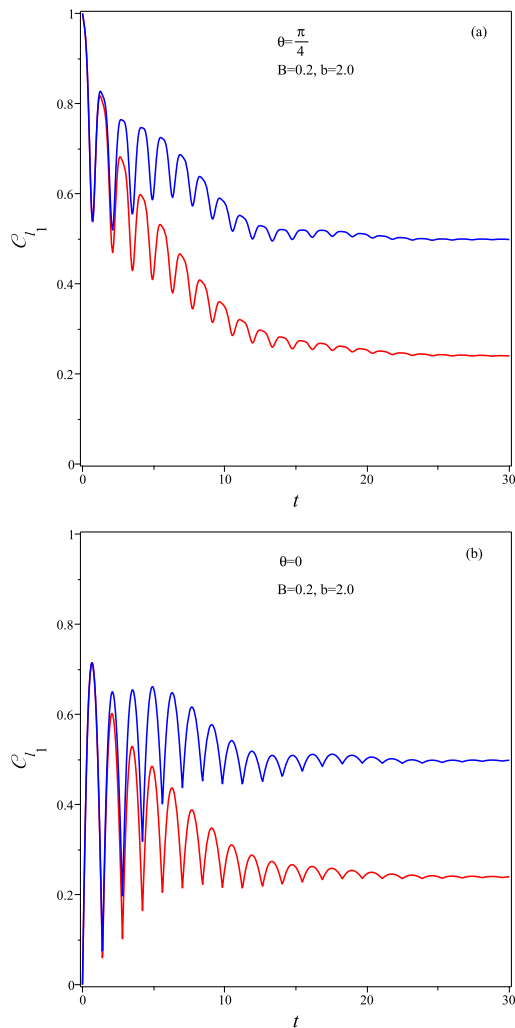


FIG. 6: (Color online) The time evolution of quantum coherence C_{l_1} for $B = 0.2$, $b = 2.0$. (a) $\theta = \frac{\pi}{4}$. (b) $\theta = 0$. The other parameters are set to $J = 2.0$, $J_0 = 1.0$, $\gamma = 0.2$, $\eta = 0.2$.

and $b = 2.0$, with fixed parameters $J = 2.0$, $J_0 = 1.0$, $\gamma = 0.2$, and $\eta = 0.2$. In Fig. 6(a), we plot the l_1 -norm of coherence, C_{l_1} , for the spin-1/2 Heisenberg XYZ chain (blue curve) and the hybrid spin-1/2 Ising-XYZ chain (red curve), a reduction in the l_1 -norm of coherence C_{l_1} is observed when the Ising interaction is included in the model. Initially, the quantum coherence in the initial state is identical in both the Heisenberg model and the Ising-XYZ hybrid model. However, as time evolves, we observe that the coherence decays more rapidly in the hybrid model compared to the original model. Subsequently, the C_{l_1} reaches the steady state after exhibiting an oscillatory behavior. In Fig. 6(b), we observe that on a short time scale for the initial unentangled state $|\Psi\rangle = |10\rangle$, the behavior of quantum coherence, captured by coherence C_{l_1} , is indistinguishable between two models. However, the norm- l_1 -norm of

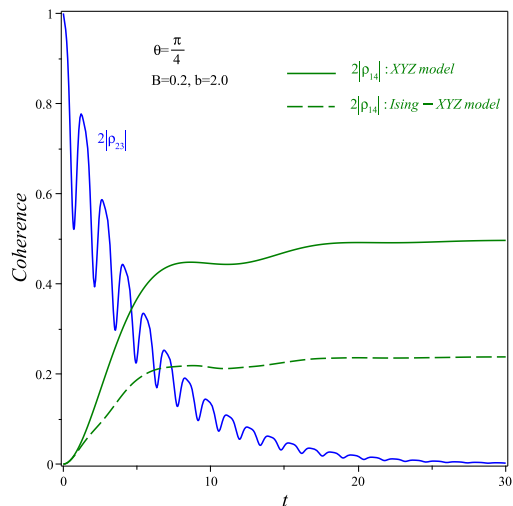


FIG. 7: (Color online) The time evolution of quantum coherence C_{l_1} for $B = 0.2$, $b = 2.0$. $\theta = \frac{\pi}{4}$. The remaining parameters are fixed at $J = 2.0$, $J_0 = 1.0$, $\gamma = 0.2$, $\eta = 0.2$.

coherence C_{l_1} in the original Heisenberg model proves to be more robust than in the hybrid Heisenberg Ising-XYZ model, both during oscillating periods and when it reaches the steady state.

In order to understand the behavior of quantum coherence C_{l_1} in the examined models, we will perform a further analysis of the components of the l_1 -norm depicted in Fig. 6(a). Thus, in Fig. 7, we can observe that the loss of quantum coherence to the environment, represented by $2|\rho_{23}|$ (blue curve), is the same in both the original model and the Ising-XYZ model. On the other hand, the quantum coherence associated with the state $2|\rho_{14}|$ returning from the environment is concentrated in the Heisenberg dimer (green curve) of the original model, while, in the case of the Ising-XYZ model, the coherence redistributes between the Heisenberg dimer and the spins with Ising-type interaction (dashed green curve). Thus, the coherence originating from environment weakens due to the dispersion of a portion of it among spin-1/2 particles with Ising-type interactions.

C. Local quantum Fisher information

The local quantum Fisher information ($LQFI$) is a crucial measure for investigating quantum correlation, particularly those of quantum discord type. In Fig. 8, we plot the ($LQFI$) and concurrence as a function of time t , using the same parameters values of Fig 2. In Fig. 8(a), we depicts the dynamics of the $LQFI$ and concurrence for the initial state $|\Psi\rangle = \frac{1}{\sqrt{2}}(|01\rangle + |10\rangle)$. It is evident that initially, the $LQFI$ aligns with the maximum concurrence of the initial state. Over time, the concurrence diminishes due to interaction with the environment, while the $LQFI$

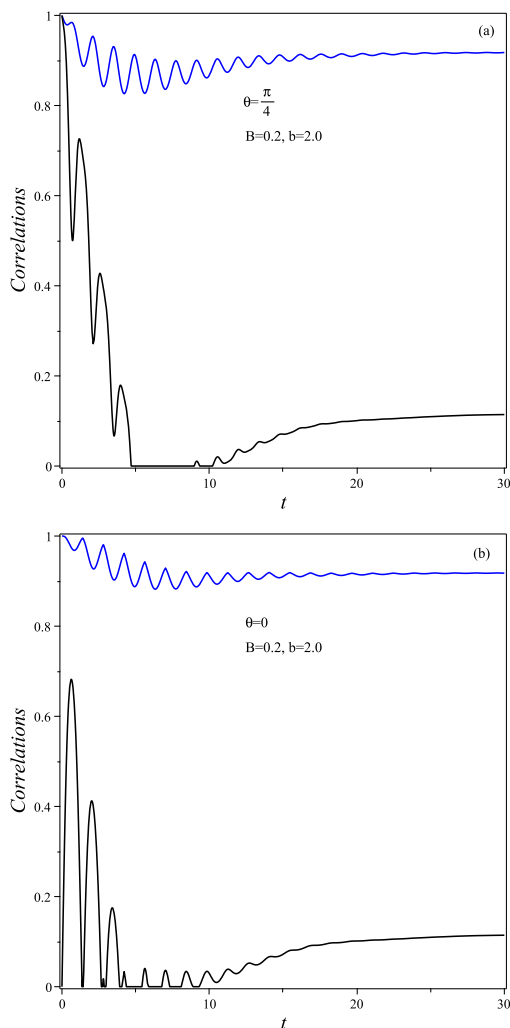


FIG. 8: (Color online) Dynamics of the correlations as a function of time t . Here the concurrence is black curve and LQFI is blue curve. (a) $B = 0.2$, $b = 2.0$, $\theta = \frac{\pi}{4}$. (b) $B = 0.2$, $b = 2.0$, $\theta = 0$. The remaining parameters are fixed at $J = 2.0$, $J_0 = 1.0$, $\gamma = 0.2$, $\eta = 0.2$.

undergoes slight oscillations before a steady state. In Fig. 8(b), we observe that, despite the qubits being initially unentangled, the correlation induced by the environment causes a sudden birth of entanglement. Following a series of sudden births and deaths of entanglement, the state eventually converges to a steady state. On the other hand, the system initially exhibits discord-like correlations quantified by the local quantum Fisher information. As time progresses, the LQFI displays a series of oscillations before converging to a steady state.

Finally, to elucidate the variations in the behavior of the l_1 -norm of coherence \mathcal{C}_{l_1} , it is important to note that the quantum coherence depends in the chosen basis. In Fig. 9, we depict the dynamics of quantum correlations (\mathcal{C} , LQFI, \mathcal{C}_{l_1}) for the same parameters as in Fig. 8(a). Remarkably, the LQFI is more robust than the coherence \mathcal{C}_{l_1} (red curve) for $\phi = 0$. This is because

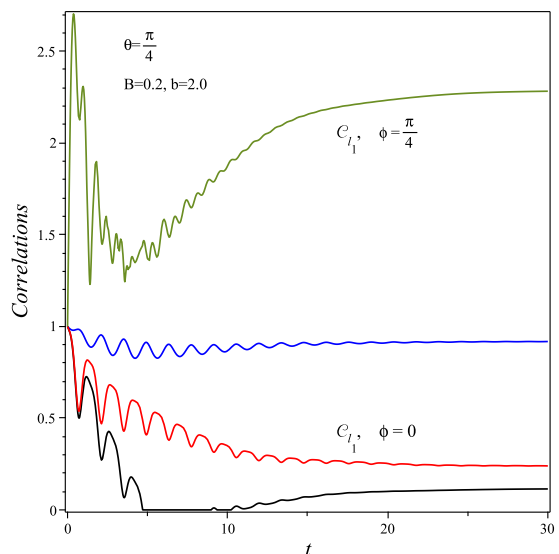


FIG. 9: (Color online) Dynamics of quantum correlations as a function of time t for the parameter $\theta = \frac{\pi}{4}$, $\phi = \frac{\pi}{4}$, $B = 0.2$ and $b = 2.0$. The other parameters are the same as those in Fig. 8.

\mathcal{C}_{l_1} , for this choice of ϕ , is composed exclusively of quantum correlations. Here, we choose $\phi = 0$ in the transformation \tilde{U} (see Eq.7) to obtain \mathcal{C}_{l_1} . However, when selecting $\phi = \pi/4$, we observe a value of \mathcal{C}_{l_1} (green curve) that exceeds both both LQFI and \mathcal{C} . This suggests that, for this particular selection of ϕ , quantum coherence incorporates quantum correlations, as well as local quantum coherences.

V. CONCLUSIONS

In this paper, we explore the impact of decoherence on the dynamics of quantum coherence in the hybrid spin-1/2 Ising-XYZ chain model with independent reservoirs at zero temperature. Furthermore, we contrast these effects with those observed in the spin-1/2 Heisenberg XYZ model [37]. When comparing the coherence dynamics between the original model and the hybrid model, the research sheds light on the intricate interaction among quantum coherence, entanglement, and environmental decoherence in spin systems. The analysis provides insights into the evolution of quantum correlations over time and their convergence to steady states under the influence of environmental factors. Particularly, the Ising interaction in the hybrid model contributes to a slight increase in entanglement compared to the original model. In contrast, when analyzing quantum coherence, we observe a reduction in coherence in the hybrid model compared to the original model. This is due to the returning coherence from the environment being redistributed between the Heisenberg dimer and the Ising spins. In addition, it is important to note that

the local quantum Fisher information has been found to be more robust than coherence in certain scenarios, highlighting the differential impact of environmental decoherence on various types of quantum correlations. In conclusion, the study emphasizes the complex nature of quantum coherence dynamics in spin systems and the significant role of environmental decoherence in shaping quantum correlations. The findings yield valuable insights into the behavior of entanglement, discord-like correlations, and coherence under environmental influences, opening opportunities for future research in quantum information processing and the dynamics of

quantum correlations.

Acknowledgment

O. Rojas, C. Filgueiras and M. Rojas thank CNPq, Capes and FAPEMIG for partial financial support. H. L. Carrion acknowledges warm hospitality during his stay at Federal University of Lavras. M. Rojas acknowledges CNPq grant 317324/2021-7 and Fapemig Grant APQ-02226-22.

-
- [1] A. Streltsov, H. Kampermann, S. Wolk, M. Gessner, D. Bruß, *New J. Phys.* **20**, 053058 (2018).
- [2] A. Streltsov, G. Adesso, M. B. Plenio, *Rev. Mod. Phys.* **89**, 041003 (2017).
- [3] Y. Yao, X. Xiao, L. Ge, C. P. Sun, *Phys. Rev. A* **92**, 022112 (2015).
- [4] C. H. Bennett, G. Brassard, C. Crepeau, R. Jozsa, A. Peres, W. K. Wootters, *Phys. Rev. Lett.* **70**, 1895 (1993).
- [5] C. H. Bennett and D. P. Di Vincenzo, *Nature* **404**, 247 (2000).
- [6] X. G. Wang, *Phys. Rev. A*, **64**, 012313 (2001); J. Maziero, H. C. Guzman, L. C. Celeri, M. S. Sarandy, R. M. Serra, *Phys. Rev. A* **82**, 012106 (2010).
- [7] T. Werlang, C. Trippe, G. A. P. Ribeiro, Gustavo Rigolin, *Phys. Rev. Lett.* **105**, 095702 (2010); G. -F. Zhang, S. -S. Li, *Phys. Rev. A* **72**, 034302 (2005).
- [8] W. Wu, J. Xu, *Phys Lett A* **381**, 239 (2017).
- [9] C. Radhakrishnan, M. Parthasarathy, S. Jambulingam, T. Byrnes, *Sci. Rep.* **7**, 13865 (2017).
- [10] G. Karpat, B. Cakmak, F. Fanchini, *Phys. Rev. B* **90**, 104431 (2014).
- [11] W. Wu, J. Xu, *Phys. Lett. A* **381**, 239 (2017).
- [12] A. Streltsov, U. Singh, H. S. Dhar, M. N. Bera, G. Adesso, *Phys. Rev. Lett.* **115**, 020403 (2015).
- [13] L. Canova, J. Strecka, M. Jascur, *J. Phys.: Condens. Matter* **18**, 4967 (2006); M. Jascur, J. Strecka, *J. Magn. Magn. Matter.* **272**, 984 (2004); O. Rojas, S. M. de Souza, V. Ohanyan, M. Khurshudyan, *Phys. Rev. B* **83**, 094430 (2011).
- [14] O. Rojas, M. Rojas, N. S. Ananikian, S. M. de Souza, *Phys. Rev. A* **86**, 042330 (2012).
- [15] W. W. Cheng, X. Y. Wang, Y. B. Sheng, L. Y. Gong, S. M. Zhao, J. M. Liu, *Sci. Rep.* **7**, 42360 (2017).
- [16] J. Torrico, M. Rojas, S. M. de Souza, O. Rojas, N. S. Ananikian, *Europhys. Lett.* **108**, 50007 (2014); J. Torrico, M. Rojas, S. M. de Souza, O. Rojas, *Phys. Lett. A* **380**, 3655 (2016); I. M. Carvalho, J. Torrico, S. M. de Souza, M. Rojas, O. Rojas, *J. Magn. Magn. Matter.* **465**, 323 (2018).
- [17] O. Rojas, M. Rojas, S. M. de Souza, J. Torrico, J. Strecka, M. L. Lyra, *Physica A* **486**, 367 (2017).
- [18] M. Rojas, S. M. de Souza, Onofre Rojas, *Ann. Phys.* **377**, 506 (2017).
- [19] I. M. Carvalho, O. Rojas, S. M. de Souza, M. Rojas, *Quantum Inf. Process.* **18**, 134 (2019).
- [20] M. Freitas, C. Filgueiras, M. Rojas, *Ann. Phys. (Berl.)* **531**, 1900261 (2019).
- [21] H. A. Zad, M. Rojas, *Physica E* **126**, 114455 (2021).
- [22] S. Kim, L. Li, A. Kumar, J. Wu, *Phys. Rev. A* **97** 032326 (2018).
- [23] M. A. Yurischev, S. Haddadi, *Phys. Lett. A* **476** 128868 (2023).
- [24] H. P. Breuer, F. Petruccione, *The Theory of Open Quantum Systems*, New York: Oxford University Press, (2002).
- [25] T. Yu, J. H. Eberly, *Phys. Rev. Lett.* **93** 140404 (2004).
- [26] L. Mazzola, S. Maniscalco, J. Piilo, K. A. Suominen, B. M. Garraway, *Phys. Rev. A* **79** 042302 (2009).
- [27] C. E. Lopez, G. Romero, MF Lastra, E. Solano, J. C. Retamal, *Phys. Rev. Lett.* **101** 080503 (2008).
- [28] J. Maziero, T. Werlang, F. F. Fanchini, L. C. Celeri, R. M. Serra, *Phys. Rev. A* **81** 022116 (2010).
- [29] L. M. Yang, B. Chen, S.-M. Fei, Z. -X. Wang, *Front. Phys.* **13** 130310 (2018).
- [30] Z. X. Man, Y. J. Zhang, F. Su, Y. J. Xia, *Eur. Phys. J. D* **58** 147 (2010).
- [31] A. G. Dijkstra, Y. Tanimura, *Phys. Rev. Lett.* **104**, 250401 (2010).
- [32] J. P. S. Peterson, T. B. Batalhao, M. Herrera, A. M. Souza, R. S. Sarthour, I. S. Oliveira, R. M. Serra, *Phys. Rev. Lett.* **123** 240601 (2019).
- [33] G. T. Landi, M. Paternostro, *Rev. Mod. Phys.* **93** 035008 (2021).
- [34] A. Manatuly, W. Niedenzu, R. Roman-Ancheyta, B. Cakmak, O. E. Mustecaplioglu, G. Kurizki, *Phys. Rev. E* **99** 042145 (2019).
- [35] T. Martin, T. A. Giresse, *Int. J. Theor. Phys.* **59** 2232 (2020).
- [36] S. Le, Y. Guo-Hui, *Chin. Phys. Lett.* **31** 030304 (2014).
- [37] C. Tao, S. Chuan-Jia, L. Jin-Xing, L. Ji-Bing, L. Tang-Kun, H. Yan-Xia, *Commun. Theor. Phys.* **53** 1053 (2010).
- [38] S. A. Hill, W. K. Wootters, *Phys. Rev. Lett.* **78**, 5022 (1997).
- [39] W. K. Wootters, *Phys. Rev. Lett.* **80**, 2245 (1998).
- [40] T. Baumgratz, M. Cramer, M. B. Plenio, *Phys. Rev. Lett.* **113**, 140401 (2014).
- [41] S. Luo, *Proc. Am. Soc.* **132**, 885 (2004).
- [42] N. Li, S. Luo, *Phys. Rev. A* **88**, 014301 (2013).
- [43] T. Yu, J. H. Eberly, *Phys. Rev. Lett.* **93**, 140404 (2004).
- [44] Z. Ficek, R. Tanas, *Phys. Rev. A* **77**, 054301 (2008).